

1 Characterizing the monomer-dimer equilibrium of  
2 UbcH8/Ube2L6: A combined SAXS and NMR  
3 study

4 *Kerem Kahraman<sup>1</sup>, Scott A. Robson<sup>2</sup>, Oktay Göcenler<sup>1</sup>, Cansu M. Yenici<sup>1</sup> Cansu D.*

5 *Tozkoparan<sup>1</sup>, Jennifer M. Klein<sup>3</sup>, Arthur L. Haas<sup>3</sup>, Joshua J. Ziarek<sup>2,\*</sup>, Çağdaş Dağ<sup>1,4,\*</sup>*

6 <sup>1</sup>Nanofabrication and Nanocharacterization Center for Scientific and Technological Advanced  
7 Research (n<sup>2</sup>STAR), Koc University, İstanbul, Turkey

8 <sup>2</sup>Department of Molecular and Cellular Biochemistry, Indiana University, 212 S. Hawthorne  
9 Drive, Bloomington, IN 47405, USA

10 <sup>3</sup>Department of Biochemistry and Molecular Biology, LSUHSC-School of Medicine, 1901  
11 Perdido Street, New Orleans, LA, 70112, USA

12 <sup>4</sup>Koc University Isbank Center for Infectious Diseases (KUISCID), Koc University, Istanbul,  
13 Turkey

14 \*Corresponding author: [cdag@ku.edu.tr](mailto:cdag@ku.edu.tr), [jjziarek@indiana.edu](mailto:jjziarek@indiana.edu)

15 KEYWORDS. ISGylation, ubiquitination, E2 enzyme, TRACT, oligomerization

16

17 **ABSTRACT:** Interferon-stimulated gene-15 (ISG15) is an interferon-induced protein with two  
18 ubiquitin-like (Ubl) domains linked by a short peptide chain, and the conjugated protein of the  
19 ISGylation system. Similar to ubiquitin and other Ubls, ISG15 is ligated to its target proteins with  
20 a series of E1, E2, and E3 enzymes known as Uba7, Ube2L6/UbcH8, and HERC5, respectively.  
21 Ube2L6/UbcH8 plays a literal central role in ISGylation, underscoring it as an important drug  
22 target for boosting innate antiviral immunity. Depending on the type of conjugated protein and the  
23 ultimate target protein, E2 enzymes have been shown to function as monomers, dimers, or both.  
24 UbcH8 has been crystalized in both monomeric and dimeric forms, but the functional state is  
25 unclear. Here, we used a combined approach of small-angle X-ray scattering (SAXS) and nuclear  
26 magnetic resonance (NMR) spectroscopy to characterize UbcH8's oligomeric state in solution.  
27 SAXS revealed a dimeric UbcH8 structure that could be dissociated when fused with an N-  
28 terminal glutathione S-transferase molecule. NMR spectroscopy validated the presence of a  
29 concentration-dependent monomer-dimer equilibrium and suggested a backside dimerization  
30 interface. Chemical shift perturbation and peak intensity analysis further suggest dimer-induced  
31 conformational dynamics at ISG15 and E3 interfaces - providing hypotheses for the protein's  
32 functional mechanisms. Our study highlights the power of combining NMR and SAXS techniques  
33 in providing structural information about proteins in solution.

34

## 35 INTRODUCTION

36 Interferon-Stimulated Gene 15 (ISG15), also known as hUCRP or IP17, is a 15 kDa ubiquitin-like,  
37 type I interferon (IFN) inducible protein [1]. ISGylation is an ubiquitin-like (Ubl) post-  
38 translational modification (PTM) that involves the covalent attachment of ISG15 to target proteins  
39 [2]. Similar to other UbIs, ISGylation plays important roles in various cellular processes such as  
40 innate antiviral immunity, protein degradation, and signal transduction [3]. Free, unconjugated,  
41 ISG15 also serves immunoregulatory functions as a cytoplasmic and secreted signaling protein in  
42 eukaryotic organisms [4]. Inherited ISG15 deficiency dramatically reduces the innate immune  
43 system's ability to fight viruses in mice yet only appears to cause immunoregulatory issues against  
44 mycobacterial, not viral diseases, in humans [3]. Thus, the role of ISG15 in human viral  
45 pathogenesis is not clearly understood.

46 The ISGylation cascade requires the sequential action of three enzymes: Ube1L as the E1 enzyme,  
47 UbcH8 as the E2 enzyme, and HERC5 as the E3 enzyme. First, ISG15 binds the catalytically active  
48 cysteine of the Ube1L activating enzyme (E1) in an ATP-dependent reaction. Then, E1 interacts  
49 with UbcH8 conjugating enzyme (E2) through its ubiquitin folding domain (UFD), which  
50 facilitates the transesterification of active ISG15, and results in an intermediate ISG15-UbcH8  
51 complex joined by a thioester bond [5]. Finally, HERC5 ligase enzyme (E3) interacts with the  
52 intermediate ISG15-UbcH8 complex to mediate ligation of ISG15 to the target protein. UbcH8  
53 plays a central role in ISGylation as it interacts with both E1 and E3 enzymes - making it a key  
54 target for the regulation of the ISGylation pathway [6].

55 Under reducing conditions, E2 enzymes can spontaneously form dimers when a crosslinker is  
56 added [7], and apart from a few exceptions, E2 enzymes are capable of preserving their dimer form

57 [8, 9]. Nevertheless, both the dimer and the monomer forms of E2 enzymes are capable of  
58 recruiting E3 enzymes and conjugating ubiquitin [10]. Although dimeric E2 enzymes are perceived  
59 as more advantageous because one of the monomers can remain associated while the ubiquitin  
60 conjugation continues with the other.

61 The Protein DataBank (PDB) contains both dimeric (PDB ID:1WZV) and monomeric (PDB  
62 ID:1WZW) crystal structures of UbcH8 (Supp. Figure 1). Yet, it is unknown whether UbcH8  
63 dimerizes naturally or as a consequence of non-specific crystal packing contacts. In this study, we  
64 aimed to characterize the oligomeric state of human UbcH8 (Ube2L6) in solution using Small  
65 Angle X-ray Scattering (SAXS). We first used a fusion protein approach with the goal of producing  
66 a high-resolution scattering envelope to properly place the UbcH8 protomers. Surprisingly, UbcH8  
67 formed stable dimers upon removal of the N-terminal fusion protein. We next used solution nuclear  
68 magnetic resonance (NMR) spectroscopy to first validate and then further characterize the  
69 monomer-dimer equilibrium. Our results indicate that UbcH8 contains a substantial dimer  
70 population at 150  $\mu$ M concentration and that dimerization may induce conformational changes at  
71 the distal ISG and E3 interaction interfaces.

## 72 **RESULTS**

73 **GST fusion guides SAXS protein structural modeling.** To determine the state of UbcH8 in  
74 solution, we expressed and purified it fused to an N-terminal glutathione-S transferase (GST) tag  
75 herein termed GST-UbcH8. We hypothesized that the 28 kDa GST molecule should be easily  
76 discernible from the smaller (18 kDa) UbcH8, and would dramatically improve fitting SAXS  
77 scattering data to the structural model. The sample was concentrated to 280  $\mu$ M and six, 10 min  
78 SAXS frames were collected for a total of one hour. Superimposition of each 10 min frame

79 confirmed that the X-ray beam produced little to no detectable radiation damage (data not shown).  
80 The medium to high  $q$  region, which is emphasized in the  $q$  vs  $I(q)$  plot, is consistent with a folded  
81 sample (Figure 1A). The Kratky plot possessed a bell-shaped curve that approaches zero after  
82 reaching a maximum at  $\sim 3$  sRg; this result is consistent with a properly folded, globular protein  
83 (Figure 1B). While slight deviations between the typical Kratky plot and dimensionless Kratky  
84 plot can aid in the assessments of flexibility, no apparent differences were observed.

85 The pair-distance distribution function,  $P(r)$ , is a measure of the frequency of interatomic  
86 distances that can also provide information about the protein shape. The presence of a shoulder in  
87 the  $P(r)$  suggests a multidomain protein as expected for the GST-UbcH8 fusion (Figure 1C). The  
88 largest distance ( $D_{\max}$ ) in the  $P(r)$  histogram was 8 nm (Figure 1C). The GST-UbcH8 crystal  
89 structures were then fitted into the final 3D DAMMIF dummy atom model (Figure 1D,E). Both  
90 GST and UbcH8 proteins, as well as the linker peptide, are clearly visible fitting a monomeric  
91 model. The fact that even the linker region can be detected with SAXS analysis and be observed  
92 this clearly, underscores the power of SAXS in structure determination. After GST cleavage,  
93 UbcH8 was observed to form a dimer based on Size Exclusion Chromatography (data not shown),  
94 hence we hypothesized that GST may block the dimerization site.

95 **FreeUbcH8 is a Dimer in Solution.** To test how well the GST-fusion improves the modeling  
96 of UbcH8 into the SAXS scattering, we prepared a second UbcH8 sample with the GST protein  
97 removed. Again, we concentrated UbcH8 to 280  $\mu\text{M}$  and collected six, 10 min frames for a total  
98 of 1 h (Figure 2A). Similar to GST-UbcH8, the Kratky plot possessed a bell-shaped curve that  
99 approaches zero (Figure 2B). We estimated a slightly larger  $R_g \sim 4.40$  nm, compared to GST-  
100 UbcH8, from the low  $q$  region, whereas the  $P(r)$   $D_{\max}$  was reduced to 6.2 nm (Figure 2C).  
101 Surprisingly, the free UbcH8  $P(r)$  also contained a shoulder suggesting homodimerization (Figure

102 2C). ATSAS molecular weight analysis predicts a 39.5 kDa particle (Supp. Table 1), which is  
103 approximately double the expected 18 kDa UbchH8. We then fitted the UbchH8 dimer crystal  
104 structure (PDB 1WZV; Figure 2D) to the dummy atom model the scattering envelope (Figure 2E).  
105 The best-fit model ( $X^2 = 1.7$ ) possesses a dimerization interface with the active site cysteines of  
106 each protomer pointed outwards (Figure 2D,E). The consistency between the previously published  
107 dimer crystal structure and the dummy atom model obtained by SAXS analysis, supports the  
108 homodimer formation of UbchH8 protein in solution in absence of a GST-tag.

109 **NMR analysis of UbchH8 monomer-dimer equilibrium.** To further establish dimerization of  
110 UbchH8 in solution, we performed Transverse Relaxation Optimized Spectroscopy (TROSY) for  
111 rotational correlation times (TRACT) experiments [11,12] to estimate the rotational correlation  
112 time ( $\tau_c$ ) of UbchH8 at two different concentrations: 300  $\mu$ M and 150  $\mu$ M (Figure 3). The signal  
113 intensity ranging from 8.6 to 9.2 ppm was integrated to maximize signal to noise and emphasize  
114 well-structured regions of the protein that are representative of global tumbling. We estimated  $^{15}$ N  
115 relaxation rates for the TROSY and anti-TROSY integrated signals using Bayesian Parameter  
116 Estimation of a two-parameter single-exponential decay model. This method produces a  
117 distribution of decay rates, which encompass uncertainty, that were then used to determine the  
118 cross-correlated relaxation (CCR) rate. The rotational correlation time was estimated from CCR  
119 according to an algebraic solution [12] of the modified Goldman relation [13], assuming an order  
120 parameter ( $O^2$ ) of 0.8. We determined a  $\tau_c \sim 16$  ns at 300  $\mu$ M and  $\sim 13$  ns at 150  $\mu$ M (Figure 3),  
121 which demonstrates a concentration dependence on molecular rotation diffusion times. We then  
122 used hydroNMR [14] to model rotational diffusion of monomeric and dimeric UbchH8 from the  
123 PDB 1WZV dimeric crystal structure. hydroNMR reported a  $\tau_c = 20.5$  ns for the dimer and 7.4 ns  
124 for the monomer at 25 °C. Taken together, this confirms that UbchH8 undergoes monomer-dimer

125 exchange and indicates a substantial dimer population even at 150  $\mu$ M. Data could not be collected  
126 at lower concentrations due to the sensitivity limit of the room temperature NMR probe.

127 We next collected  $^{15}$ N heteronuclear single quantum coherence (HSQC) solution NMR spectra  
128 at 150  $\mu$ M and 300  $\mu$ M to identify UbcH8's dimerization interface. Resonances were assigned by  
129 visual inspection using BMRB Entry ID 16321 as a reference list. The NH resonances of all  
130 residues except for the 18 prolines were assigned (79.85% completion). We then assessed both  
131 concentration-dependent chemical shift perturbations (CSPs) and peak intensity differences. The  
132 concentration-dependent CSPs were of relatively low magnitude and located far from the  
133 crystallographic dimerization interface (Figure 4). All of the perturbed residues except for N23,  
134 which resides at the dimerization site, are situated at either the E1 or the ISG15 interaction surfaces.  
135 Residues E80, N81, and G82 are clustered on a loop near the catalytic C85 residue where ISG15  
136 is covalently attached. Whereas F56, K99, V103, L104, and N108 are proximal to the E1 binding  
137 region on the UbcH8 surface; interestingly, these residues are arranged towards the UbcH8 core  
138 rather than at the surface (Figure 4). Given that ISG15 and E1 involve distinct interfaces, we  
139 hypothesize a conformational change or allosteric pathway influences the transfer or binding of  
140 ISG15. Our results suggest that dimerization may play an additional role in ISGylation. We  
141 hypothesize that the weak CSPs could reflect a mostly sidechain-mediated interface and/or that the  
142 ensemble is predominantly dimeric even at 150  $\mu$ M concentration.

143 Thus, we also measured the concentration-dependent changes in peak intensity. We hypothesize  
144 these intensity differences result from monomer-dimer exchange on the intermediate  
145 (microsecond-millisecond) timescale, but it's also possible that they reflect dimerization-  
146 dependent fluctuations in longitudinal ( $T_1$ ) or transverse ( $T_2$ ) relaxation. The largest changes in  
147 peak intensity again clustered to the ISG15 and E1 interfaces, while also highlighting an extended

148 region along the crystalized dimer interface (Figure 5). D149 sits at the center of the dimerization  
149 surface with E141 and L144 in close proximity. It's plausible that D28 and A29, located in a loop  
150 region of the opposing protomer, could possess the flexibility to interact. Furthermore as the  
151 overall structure gets bigger with the dimerization, decreased signals from some peaks were  
152 expected due to line broadening. Although unlike the CSP analysis which showed that most of the  
153 conformational changes occurred away from the dimerization site, delta chemical shift intensity  
154 analysis revealed that most of the affected residues were on the dimerization site. In fact, the peak  
155 intensity of N23 and D149 residues (Supp. Figure 2) from opposing protomers, which are within  
156 3.3 Å distance in the crystal structure, deviated from the mean peak height by 44.7% and 62.2%,  
157 at 150µM, and 37.6% and 35.6%, at 300 µM, respectively. Taken together, this indicates that  
158 dimerization is *ipso facto* involved in defining interaction dynamics between E1 and E2 enzymes.

## 159 **DISCUSSION**

160 In this study, we investigated the oligomeric state of UbcH8 in solution using Small Angle X-ray  
161 Scattering (SAXS) and NMR analysis. To improve the fitting of SAXS scattering data to the  
162 structural model, we initially employed an N-terminal GST-fused UbcH8 protein. The results from  
163 SAXS experiments and analysis indicate that the GST-UbcH8 fusion protein is monodisperse and  
164 properly folded in solution. The 3D DAMMIF dummy atom model also revealed a monomeric  
165 model of the GST-UbcH8 fusion protein, highlighting the advantages of SAXS in structure  
166 determination. The free form of UbcH8, without the GST fusion, was further investigated.  
167 Surprisingly, the P(r) distribution suggested a multidomain complex, and the ATSAS molecular  
168 weight analysis indicated dimer formation. The consistency between the existing crystal structure  
169 of UbcH8 dimer and the SAXS-derived dummy atom model supports the formation of a UbcH8  
170 homodimer in solution in the absence of a GST-tag.



171 Our NMR analysis, including chemical shift perturbation and peak intensity measurements,  
172 provide additional evidence for the dimerization of UbcH8. Residues involved in the dimerization  
173 process were identified, and the effects of dimerization on the E1 and ISG15 interaction sites were  
174 observed. The TRACT experiments also supported the dimerization of UbcH8, revealing a  
175 concentration-dependent behavior of UbcH8 in solution, which suggests monomer-dimer  
176 exchange on an intermediate timescale. The dimerization of UbcH8 and its implications on the  
177 ISGylation process are consistent with previous reports of E2 enzymes forming dimers to facilitate  
178 polyubiquitination [10]. Dimerization of several E2 enzymes are reported and the observed  
179 dimerization of the enzymes are found to be stimulating the catalytic activity of the E2 enzyme in  
180 these studies [9,15,16,17]. In 2010, David et. al. suggested that E2 enzymes form dimers in  
181 solution regardless if an active ubiquitin is present [7]. While the monomer form is also active for  
182 the acquisition of the ubiquitin, dimer form of the E2 is found to be more advantageous as while  
183 one monomer site is binding the ubiquitin molecules, the other site is capable of remaining  
184 associated to the target protein and thus facilitates efficient polyubiquitination. The acting  
185 mechanism of E2 enzymes proposed in this study suggests that the E2 enzymes function as dimers  
186 while catalyzing polyubiquitination process [7]. Our results demonstrate that UbcH8, the E2  
187 enzyme specific for ISGylation, can also form dimers at near physiological concentrations. This  
188 suggests that the ISGylation process may also involve dimerization for regulating the complicated  
189 interactions of E1, E2 and E3 enzymes. This study highlights the importance of understanding the  
190 oligomeric state and behavior of proteins in solution to gain insights into their biological function  
191 and regulation. Moreover, our work emphasizes the usefulness of SAXS and NMR techniques in  
192 elucidating protein structures and interactions in solution, which can complement crystallographic  
193 studies and provide a more biologically relevant context.

194 Future studies may focus on exploring the functional implications of UbcH8 dimerization in the  
195 ISGylation process, such as the effects on substrate specificity, E1 and E3 enzyme interactions,  
196 and the kinetics of ISGylation. Additionally, the molecular mechanisms underlying the observed  
197 concentration-dependent behavior of UbcH8 and the role of post-translational modifications in  
198 modulating its oligomeric state could be investigated further. These studies will contribute to a  
199 more comprehensive understanding of the regulation and function of UbcH8 in the context of  
200 ISGylation and its broader implications in various diseases, including viral and bacterial infections,  
201 cancer, and autoimmune disorders.

202

## 203 **MATERIALS AND METHODS**

204 **Protein expression and purification.** Three alanine residues followed by the coding sequence  
205 of the UbcH8 protein are inserted in the 5' BamH1/ 3' EcoR1 restriction sites of the pGEX-4T3  
206 plasmid. Three alanine residues are inserted between the GST and UbcH8 protein sequence in  
207 order to increase the binding efficiency and also to provide a better cleavage upon thrombin  
208 treatment during the purification of the protein sample. The final coded amino acid sequence  
209 was: MSPILGYWKIKGLVQPTRLLEYLEEKYEEHLYERDEGDKWRNKKFELMGLEFPNL  
210 PYYIDGDVKL TQSMAIIRYIADKHNMLGGCPKERA EISMLEGAVLDIRYGVSRIA YSKDF  
211 ETLKVDFLSKLPEMLKMFEDRLCHKTYLNGDHVTHPDFMLYDALDVVLYMDPMCLDA  
212 FPKLVCFKKRIE AIPQIDKYLKSSKYIAWPLQG WQAFGGGDHPPKSDLVPRGSAAAMAS  
213 MRVVKELEDLQKKPPPYLRNLSSDDANVLVWHALLLPDQPPYHLKAFNLRISFPPEYPF  
214 KPPMIKFTTKIYHPNVDENGQICLPIISSENWKPCTKTCQVLEALNVLVNRPNIREPLRMD  
215 LADLLTQNPELFRKNAEEFTLRFGVDRPS\*

216 pGEX-4T3 GST-AAA-UbcH8 plasmid was transformed into Rosetta2 *E. Coli* expression cells,  
217 plated on LB-ampicillin-chloramphenicol, and grown overnight at 37 °C. The next morning,  
218 colonies were picked from the agar plate and inoculated into 10 ml LB-ampicillin-chloramphenicol  
219 medium. The culture was grown overnight at 37 °C at 110 rpm. The overnight culture was  
220 transferred into 1 L LB medium and incubated at 37°C. After OD<sub>595</sub> exceeded 0.3, temperature  
221 was lowered to 18°C and protein production was induced at OD<sub>595</sub> 0.8 by the addition of 0.4mM  
222 IPTG. Cells were harvested 18 hours after induction by centrifugation at 2000 RCF for 1 hour.

223 Harvested cells were resuspended in lysis buffer (500mM NaCl, 50mM Tris, 0.1% (v/v) Triton X-  
224 100, 5% (v/v) glycerol, 1mM DTT, pH=7.5), sonicated, and centrifuged at 20K RCF for 1 hour to  
225 remove insoluble debris. The obtained supernatant was loaded to a GST affinity column  
226 equilibrated with 20mM Tris (pH 7.5), 150mM NaCl, 1mM DTT. Non-specific proteins were  
227 washed with the same buffer and the protein was eluted with 30mM glutathione, 20mM Tris (pH  
228 7.5), 150mM NaCl, 1mM DTT. For cleavage of the GST tag, 1:100 thrombin enzyme was added  
229 to the eluted protein and dialyzed in 20mM Tris (pH 7.5), 150mM NaCl, 1mM DTT solution  
230 overnight to eliminate excess glutathione. For separation of the GST tag, reverse GST  
231 chromatography was applied. Unbound free UbcH8 was collected and purified by size exclusion  
232 chromatography using 20mM Tris (pH 7.5), 150mM NaCl, 1mM DTT buffer.

233

234 **SAXS Data Collection.** All SAXS data were collected at home source SAXSpoint 5.0 (Anton  
235 Paar GmbH) as described before [18]. Sample/detector distance (SDD) was 1600 mm for SAXS  
236 experiments. All measurements took place at 10 °C. Data was collected in one hour session(1-  
237 minutes long 6 frames) for each measurement. The scattering curves were checked for radiation

238 damage and no damage was detected after the superimposition of each 10 minute data collection  
239 intervals..

240 **SAXS Data Processing and Modeling.** At first, the scattering pattern of all samples were  
241 visually inspected in the Primus program of ATSAS 3.0 for any possible issues with the  
242 measurement[11]. The radius of gyration ( $R_g$ ) was calculated using Guinier's equation and inverse  
243 Fourier transform by Primus. Distance distribution function  $P(r)$  and the maximum particle  
244 diameter ( $D_{max}$ ) was calculated by GNOM[19]. After estimating the molecular weight of the  
245 model DAMMIF (ab initio) is used to generate 5 independent low resolution models from the data.  
246 [20]. DAMAVER and DAMMIN then averaged, clustered, and optimized these 5 distinct solutions  
247 to form the final ab-initio shape [21]. SASpy plug-in for PyMOL was used to superimpose the  
248 homology modeled structure of the protein [22, 23].

249  **$^{15}N$  Labeled Protein Expression and Purification.** pGEX-4T3 GST-AAA-UbcH8 plasmid  
250 containing bacteria were grown overnight in LB medium at 37°C and transferred into 50 mL  $^{15}N$   
251 labeled M9 media the next day. Following 4 hours of incubation at 37°C, cells were transferred  
252 into 1L M9 media. After  $OD_{595}$  exceeded 0.3, temperature was lowered to 18°C and protein  
253 production was induced at  $OD_{595}$  0.8 by the addition of 0.4mM IPTG. The medium contained  
254 33.7mM  $Na_2HPO_4$ , 22 mM  $KH_2PO_4$ , 8.55 mM NaCl, 9.35 mM  $^{15}N$  labeled  $NH_4Cl$ , 1mM  $MgCl_2$ ,  
255 0.3mM  $CaCl_2$ , and 7 mg/L  $FeCl_2 \cdot 4H_2O$ . Cells were harvested 18 hours after induction by  
256 centrifugation at 2000 RCF for 1 hour.

257 Harvested cells were resuspended in lysis buffer (500mM NaCl, 50mM Tris, 0.1% (v/v) Triton X-  
258 100, 5% (v/v) glycerol, 1mM DTT, pH=7.5), sonicated, and centrifuged at 20K RCF for 1 hour to  
259 remove insoluble debris. The obtained supernatant was loaded to a GST affinity column

260 equilibrated with 38.39 mM Na<sub>2</sub>HPO<sub>4</sub>, 11.61 mM KH<sub>2</sub>PO<sub>4</sub> (pH 7.4), 100 mM NaCl, 1mM DTT.  
261 Non-specific proteins were washed with the same buffer and the protein was eluted with 30mM  
262 glutathione, 38.39 mM Na<sub>2</sub>HPO<sub>4</sub>, 11.61 mM KH<sub>2</sub>PO<sub>4</sub> (pH 7.4), 100 mM NaCl, 1mM DTT. For  
263 cleavage of the GST tag, 1:100 thrombin enzyme was added to the eluted protein and dialyzed in  
264 38.39 mM Na<sub>2</sub>HPO<sub>4</sub>, 11.61 mM KH<sub>2</sub>PO<sub>4</sub> (pH 7.4), 100 mM NaCl, 1mM DTT solution overnight  
265 to eliminate excess glutathione. For separation of the GST tag, reverse GST chromatography was  
266 applied. Unbound free Ubch8 was collected and purified by size exclusion chromatography using  
267 38.39 mM Na<sub>2</sub>HPO<sub>4</sub>, 11.61 mM KH<sub>2</sub>PO<sub>4</sub> (pH 7.4), 100 mM NaCl, 1mM DTT buffer.

268

269 **NMR Data Acquisition and analysis.** The protein was concentrated to 0.287 mM. 10% D<sub>2</sub>O  
270 (final concentration) containing 1mM DSS was added to obtain a final sample volume of 600 μL.  
271 All NMR data acquisition process was completed using 500 MHz Bruker Ascend magnet equipped  
272 with Avance NEO console and BBO double resonance room temperature probe at Koç University  
273 n<sup>2</sup>STAR NMR Facility. 2-D <sup>1</sup>H-<sup>15</sup>N HSQC spectra were recorded with 50% non-uniform sampling  
274 (NUS) at 298 K with a <sup>1</sup>H spectral width of 14 ppm (1024 data points in t<sub>2</sub>) and a <sup>15</sup>N spectral  
275 width of 32 ppm (64 data points in t<sub>1</sub>). The 2D data was processed by NMRPipe [24] and analyzed  
276 using NMRFAM-SPARKY [25]. The combined <sup>1</sup>H-<sup>15</sup>N chemical shift perturbations were  
277 calculated using equation  $\Delta\delta_{AV} = [(\Delta\delta^{1H})^2 + (\Delta\delta^{15N} * 0.14)^2]^{1/2}$  [26].

278 1D TRACT experiments [11] were collected with 1024 complex points and 1.5 s recycle delay.  
279 Relaxation rates for <sup>15</sup>N TROSY and anti-TROSY components were determined from spectra  
280 intensity values integrated over 9.2 to 8.6 ppm at eight relaxation delays: 30, 60, 90, 120, 150, 180,  
281 210, 240, 270 and 300 ms. Each relaxation rate and its uncertainty was estimated by fitting the

282 integrated values and time delays to a single parameter exponential decay model using Bayesian  
283 Parameter Estimation. Each TROSY and anti-TROSY relaxation rate was then used to estimate  
284 rotational correlation time ( $\tau_c$ ) using the algebraic method [12] where we assumed an order  
285 parameter ( $O^2$ ) of 0.8.

## 286 **Author Contributions**

287 **Çağdaş Dağ:** Conceptualization, Methodology, Supervision Funding acquisition, Writing-  
288 Reviewing and Editing, Writing-Original draft preparation **Joshua J. Ziarek:** Conceptualization,  
289 Writing- Reviewing and Editing, Writing- Original draft preparation **Arthur L. Haas:**  
290 Conceptualization, Supervision **Kerem Kahraman:** Investigation, Formal analysis, Visualization,  
291 Writing- Reviewing and Editing, Writing- Original draft preparation. **Scott A. Robson:**  
292 Investigation, Formal analysis, Visualization, Writing- Reviewing and Editing **Oktay Göcenler:**  
293 Formal analysis, Investigation Writing - Original Draft, Visualization **Cansu M. Yenici:**  
294 Investigation, Visualization, Formal analysis. **Cansu D. Tozkoparan:** Visualization, Formal  
295 analysis **Jennifer M. Klein:** Investigation.

## 296 **ACKNOWLEDGMENT**

297 CD acknowledges support from TÜBİTAK (Project No: 120Z594, 122Z747). JJZ acknowledges  
298 support from National Institutes of Health grant R35GM143054. The authors acknowledge the use  
299 of the services and facilities of n<sup>2</sup>STAR-Koç University Nanofabrication and Nanocharacterization  
300 Center for Scientific and Technological Advanced Research.

301

302 **REFERENCES**

303 [1] Haas, A. L., Ahrens, P., Bright, P. M., Ankel, H. (1987) Interferon induces a 15-kilodalton  
304 protein exhibiting marked homology to ubiquitin. *Journal of Biological Chemistry*, 262(23),  
305 11315-11323.

306 [2] Loeb, K. R., Haas, A. L. (1992) The interferon-inducible 15-kDa ubiquitin homolog conjugates  
307 to intracellular proteins. *Journal of Biological Chemistry*, 267(11), 7806-7813.

308 [3] Perng, YC., Lenschow, D.J. (2018) ISG15 in antiviral immunity and beyond. *Nat Rev*  
309 *Microbiol* 16, 423–439

310 [4] Swaim CD, Scott AF, Canadeo LA, Huibregtse JM. (2017) Extracellular ISG15 Signals  
311 Cytokine Secretion through the LFA-1 Integrin Receptor. *Mol Cell*, 68(3):581-590

312 [5] Durfee, L. A., Kelley, M. L., Huibregtse, J. M. (2008) The basis for selective E1-E2  
313 interactions in the ISG15 conjugation system. *Journal of Biological Chemistry*, 283(35), 23895-  
314 23902.

315 [6] Stewart, M. D., Ritterhoff, T., Klevit, R. E., Brzovic, P. S. (2016) E2 enzymes: more than just  
316 middle men. *Cell research*, 26(4), 423-440.

317 [7] David, Y., Ziv, T., Admon, A., Navon, A. (2010) The E2 ubiquitin-conjugating enzymes direct  
318 polyubiquitination to preferred lysines. *Journal of Biological Chemistry*, 285(12), 8595-8604.

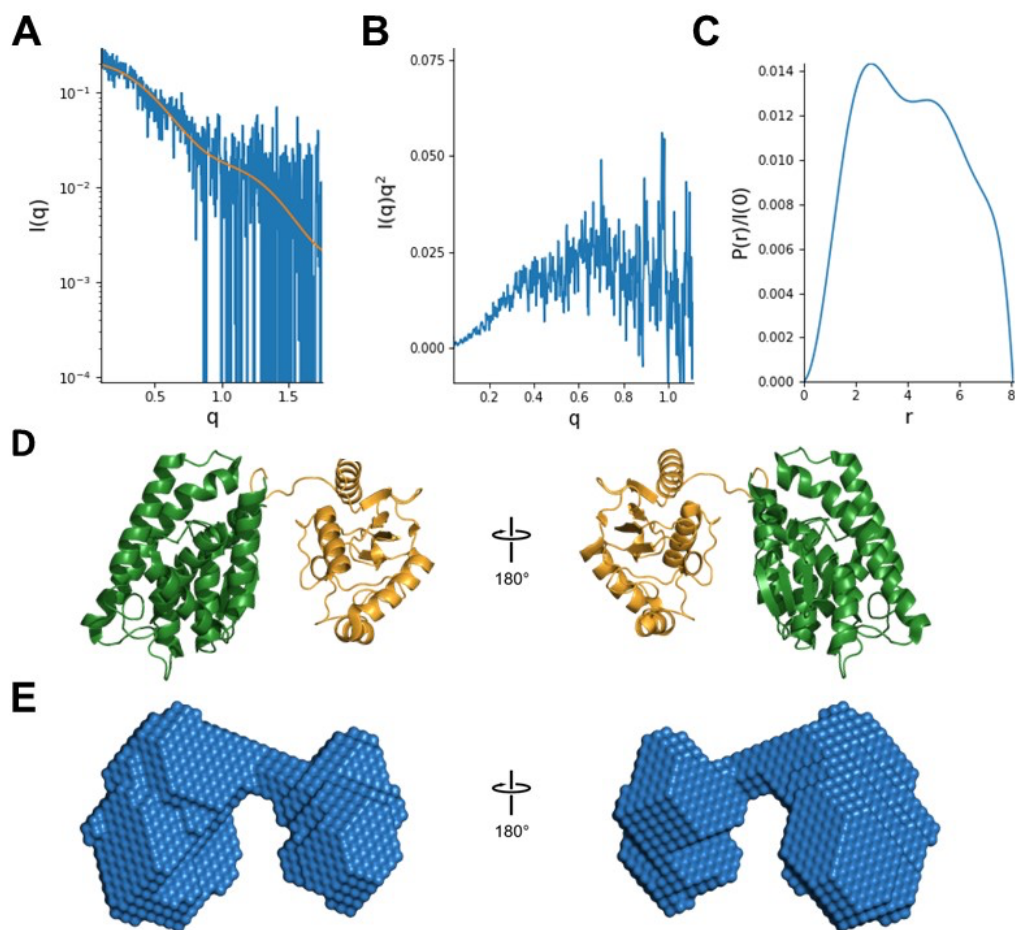
319 [8] Vittal, V., Wenzel, D. M., Brzovic, P. S., Klevit, R. E. (2013). Biochemical and structural  
320 characterization of the ubiquitin-conjugating enzyme UBE2W reveals the formation of a  
321 noncovalent homodimer. *Cell biochemistry and biophysics*, 67(1), 103-110.

- 322 [9] Liess, A. K., Kucerova, A., Schweimer, K., Schlesinger, D., Dybkov, O., Urlaub, H., ... &  
323 Lorenz, S. (2020) Dimerization regulates the human APC/C-associated ubiquitin-conjugating  
324 enzyme UBE2S. *Science signaling*, 13(654), eaba8208.
- 325 [10] Bremm, A. (2020) Hug and hold tight: Dimerization controls the turnover of the ubiquitin-  
326 conjugating enzyme UBE2S. *Science Signaling*, 13(654), eabd9892.
- 327 [11] Lee, D., Hilty, C., Wider, G., Wuthrich, K. (2006) Effective rotational correlation times of  
328 proteins from NMR relaxation interference. *J Magn Reson* 178, 72–6.
- 329 [12] Robson, S. A., Dağ, Ç. Wu, H., Ziarek, J. J. (2021) *Journal of Biomolecular NMR* volume  
330 75, 293–302.
- 331 [13] Goldman, M. (1984) Interference effects in the relaxation of a pair of unlike spin-12 nuclei.  
332 *Journal of Magnetic Resonance* 60, 437–452.
- 333 [14] J García de la Torre, M.L Huertas, B Carrasco (2000) HYDRONMR: Prediction of NMR  
334 Relaxation of Globular Proteins from Atomic-Level Structures and Hydrodynamic Calculations,  
335 *Journal of Magnetic Resonance*, 147, 1.
- 336 [15] Liu, W., Shang, Y., Zeng, Y., Liu, C., Li, Y., Zhai, L., ... Li, W. (2014) Dimeric Ube2g2  
337 simultaneously engages donor and acceptor ubiquitins to form Lys48-linked ubiquitin chains. *The*  
338 *EMBO journal*, 33(1), 46-61.
- 339 [16] Li, W., Tu, D., Brunger, A. T., Ye, Y. (2007). A ubiquitin ligase transfers preformed  
340 polyubiquitin chains from a conjugating enzyme to a substrate. *Nature*, 446(7133), 333-337.



- 341 [17] Varelas, X., Ptak, C., Ellison, M. J. (2003). Cdc34 self-association is facilitated by ubiquitin  
342 thiolester formation and is required for its catalytic activity. *Molecular and cellular biology*,  
343 23(15), 5388-5400.
- 344 [18] Göcenler, O. , Yenici, C. M. , Kahraman, K. , Büyükdağ, C. & Dağ, Ç. (2022). Biomolecular  
345 Solution X-Ray Scattering At n2STAR Beamline. *Mugla Journal of Science and Technology* , 8  
346 (2) , 60-69
- 347 [19] Svergun, D.I. (1992) Determination of the regularization parameter in indirect-transform  
348 methods using perceptual criteria. *J. Appl. Crystallogr.* 25, 495-503.
- 349 [20] Franke, D., Svergun, D.I. (2009) DAMMIF, a program for rapid ab-initio shape determination  
350 in small-angle scattering. *J. Appl. Cryst.*, 42, 342-346.
- 351 [21] D. I. Svergun, D. I. (1999) Restoring low resolution structure of biological macromolecules  
352 from solution scattering using simulated annealing. *Biophys J.* 2879-2886.
- 353 [22] Schrödinger, L., DeLano, W. (2020) PyMOL. Retrieved from <http://www.pymol.org/pymol>.
- 354 [23] Panjkovich, A., Svergun, D. I. (2016) SASpy: a PyMOL plugin for manipulation and  
355 refinement of hybrid models against small angle X-ray scattering data. *Bioinformatics*, 32(13),  
356 2062-2064.
- 357 [24] Delaglio, F., Grzesiek, S., Vuister, G.W. Zhu, G., Pfeifer, J., Bax, A. (1995) *J. Biomol.*  
358 *NMR.* 6, 277-293.
- 359 [25] Lee, W., Tonelli, M., Markley, J. L. (2015) NMRFAM-SPARKY: enhanced software for  
360 biomolecular NMR spectroscopy. *Bioinformatics (Oxford, England)*, 31(8), 1325–1327.

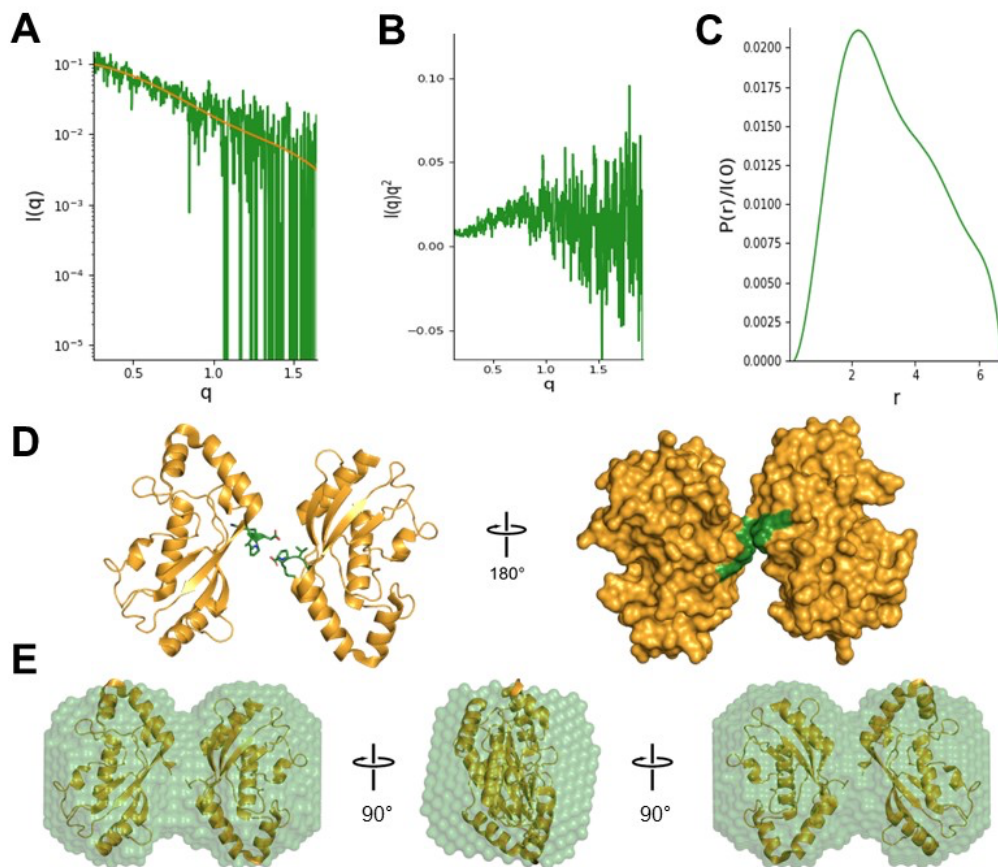
- 361 [26] Williamson, M. P. (2013) Using chemical shift perturbation to characterise ligand binding,  
362 Progress in Nuclear Magnetic Resonance Spectroscopy, 73, 1-16.  
363



364

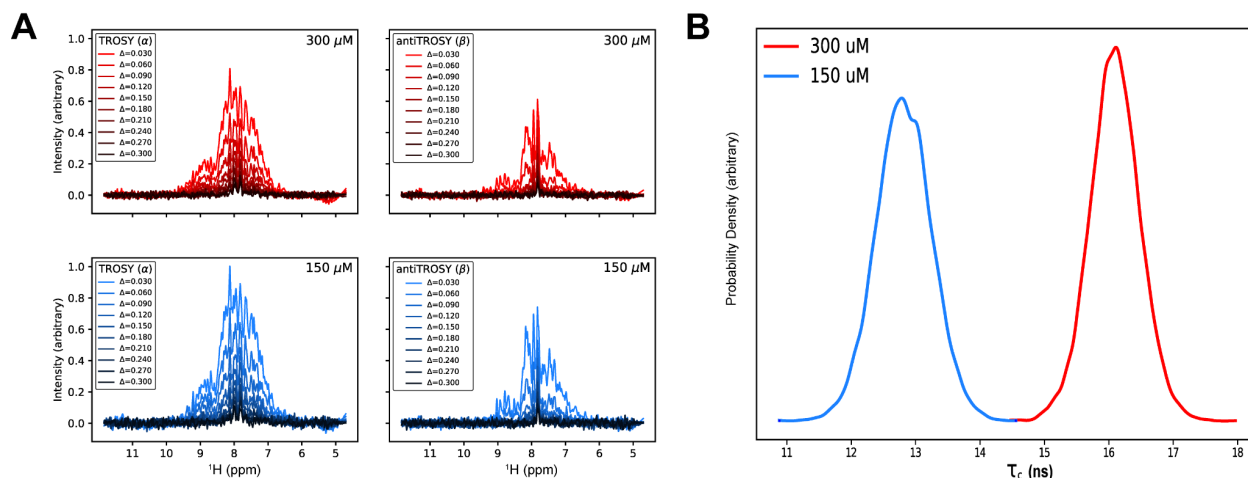
365 **Figure 1. SAXS analysis of GST-UbcH8 fusion protein.** (A)  $\ln I(s)$  vs  $s$  plot, (B) Kratky plot,  
366 and (C) Pair distance distribution,  $P(r)$ , plot of the experimental SAXS intensity obtained at 4.1  
367 mg/ml (280  $\mu$ M) of the GST-UbcH8 fusion protein. The pair-distance distance distribution plot of  
368 the GST-UbcH8 fusion protein scattering data calculated by GNOM. (D) The individual crystal  
369 structures of GST (PDB:1R5A) and UbcH8 (PDB:1WZW) shown as cartoon representations. (E)  
370 The GST-UbcH8 dummy atom model, obtained by the ATSAS online package, is shown as a  
371 surface representation.

372



373

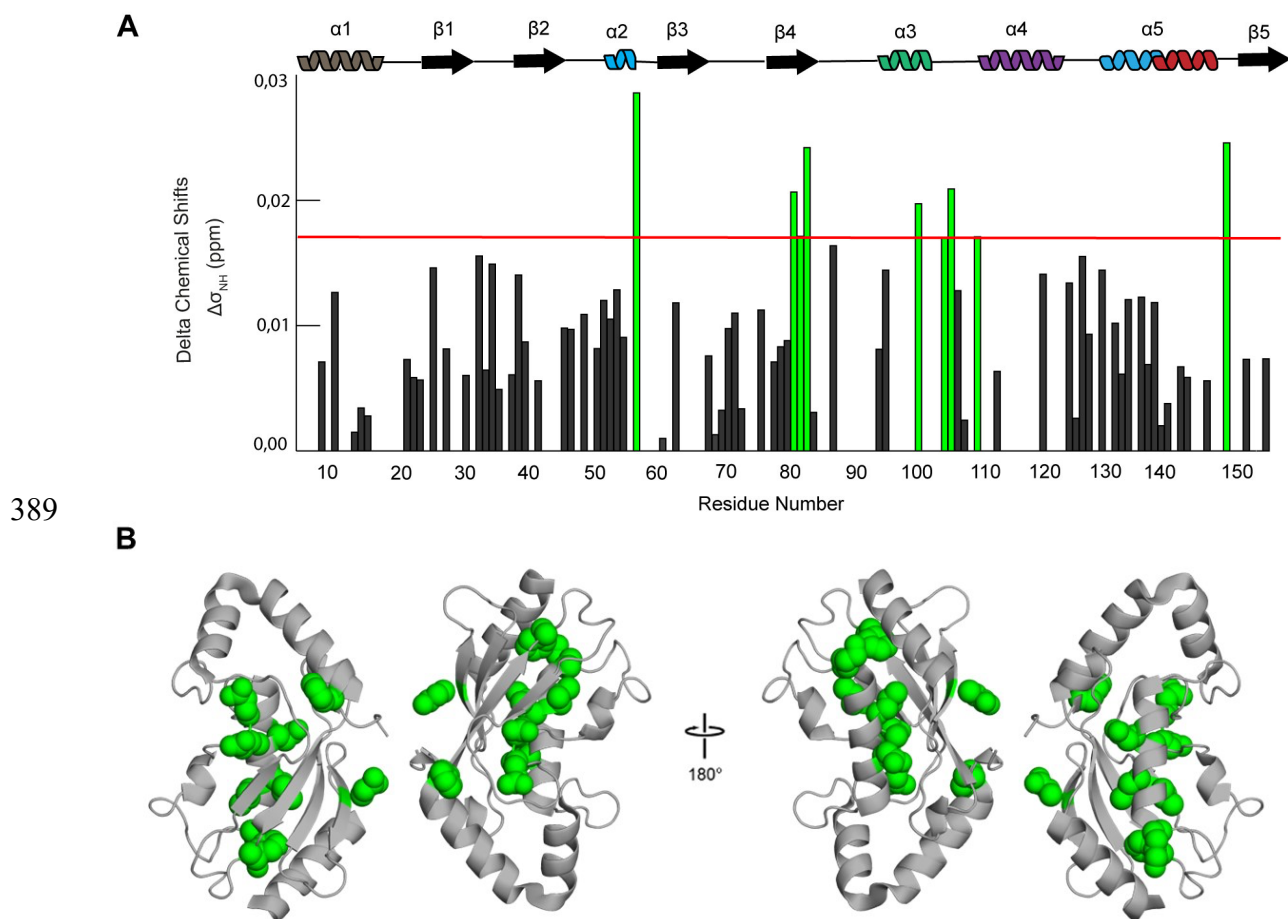
374 **Figure 2. SAXS analysis of free UbchH8.** (A)  $\ln I(s)$  vs  $s$  plot, (B) Kratky plot, and (C) Pair  
375 distance distribution,  $P(r)$ , plot of the experimental SAXS intensity obtained at 4.1 mg/ml (280  
376  $\mu\text{M}$ ) free UbchH8 protein. (D) Crystal structure of UbchH8 dimer (pdb:1WZV) shown as cartoon  
377 and surface representation using Pymol. Residues D149, R150, and P151 of the dimerization  
378 interface are colored forest green. (E) UbchH8 dimer crystal structure (pdb:1WZV) fitted ( $\chi = 1.02$ )  
379 into the DAMMIF dummy atom model using SASpy.



380

381 **Figure 3. TRACT analysis of free UbCh8 to determine rotational correlation time.** (A) The  
382 UbCh8 1D <sup>15</sup>N TROSY (left) and anti-TROSY (right) spectra from the TRACT experiment. The  
383 top and bottom panels are UbCh8 at 300 (red) and 150 μM (blue), respectively. We integrate from  
384 8.6-9.2 ppm (gray boxed region) under the assumption that it possesses resonances from primarily  
385 structured regions. (B) The probability density estimates of the overall rotational correlation time  
386 ( $\tau_c$ ) for UbCh8 at 300 μM (red) and 150 μM (blue). The average (point) estimate for 300 μM and  
387 150 μM UbCh8 are 16.1 ns and 12.8 ns, respectively.

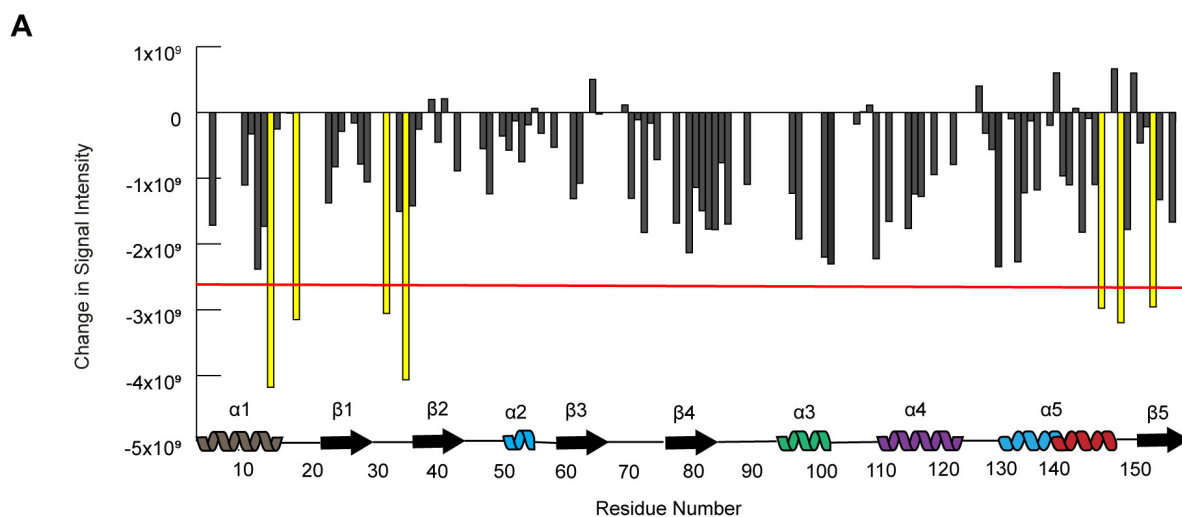
388



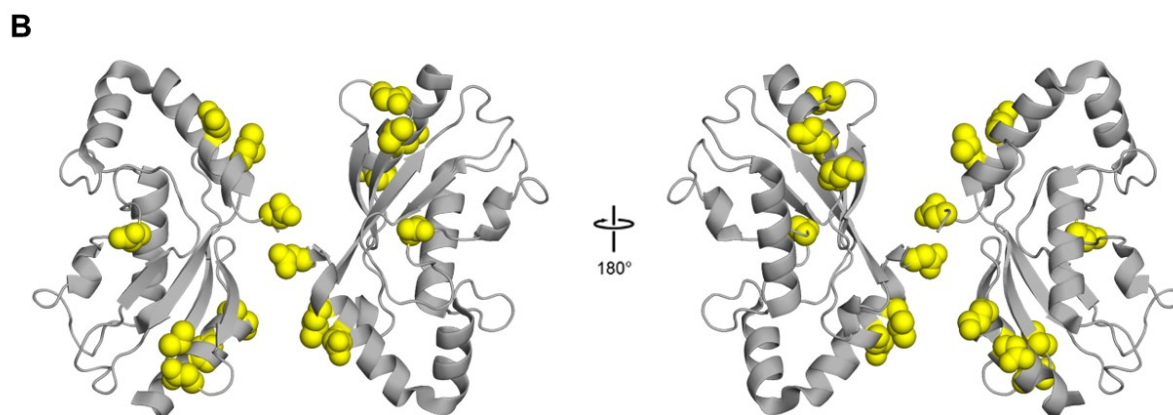
389

390

391 **Figure 4.  $^1\text{H}$ - $^{15}\text{N}$  Chemical shift perturbations mapped onto UbcH8 dimeric crystal**  
392 **structure.** A) The combined  $^1\text{H}$ - $^{15}\text{N}$  chemical shift perturbations between 300  $\mu\text{M}$  and 150  $\mu\text{M}$   
393 UbcH8 were calculated for each residue. The residues colored green possessed chemical shift  
394 perturbations larger than the threshold (red line). Residues with no bars were not observed at either  
395 concentration. B) Residues with chemical shift perturbations larger than the threshold were  
396 mapped onto the UbcH8 dimeric crystal structure (PDB 1WZV). These residues cluster to three  
397 distinct regions: the dimer interface (N23), the ISG15 conjugation site (E80, N81, and G82), and  
398 the E1 binding surface (F56, K99, V103, L104, and N108).



399



400

401 **Figure 5. Concentration dependent chemical shift signal intensity changes** A) Concentration-  
402 dependent changes in  $^1\text{H}$ - $^{15}\text{N}$  peak intensity mapped onto UbcH8 dimeric crystal structure. The  
403 residues colored yellow possessed peak intensity changes that were larger than the threshold (red  
404 line); these residues are D12, K16, N30, V33, E141, L144, and D149. Residues with no bars were  
405 not observed at either concentration. B) Residues with peak intensity changes larger than the  
406 threshold were mapped onto the UbcH8 dimeric crystal structure (PDB 1WZV).

407





409 **SUPPLEMENTARY INFORMATION**

410

411 **Supplementary Table 1.** Molecular Size Parameters of GST-UbcH8 and UbcH8 dimer Obtained  
412 from SAXS Data Analysis.

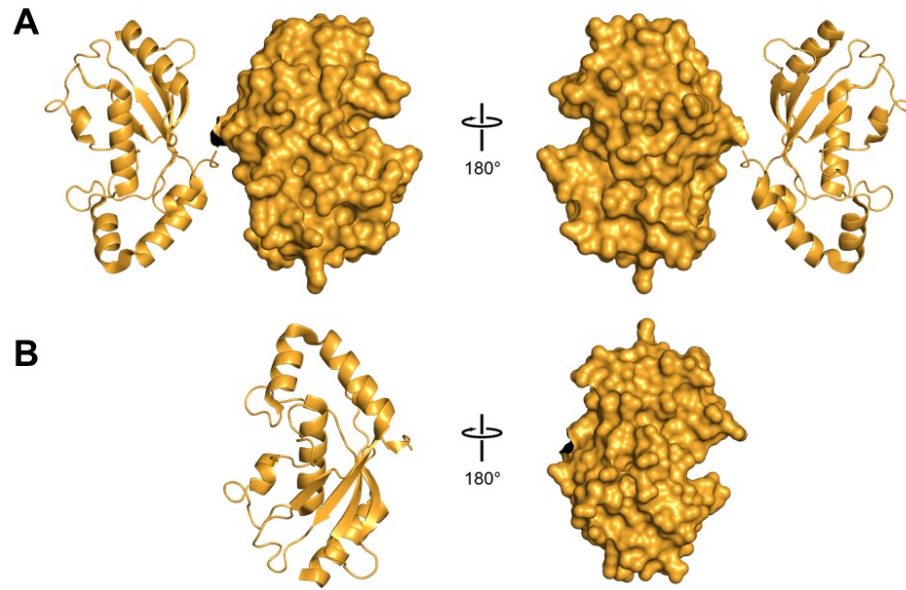
Sample	R <sub>g</sub> (nm) <sup>a</sup>	D <sub>max</sub> (nm) <sup>b</sup>	V <sub>p</sub> (Å <sup>3</sup> ) <sup>c</sup>	MW (kDa) <sup>d</sup>	V <sub>c</sub> (kDa) <sup>e</sup>	Q <sub>p</sub> (kDa) <sup>f</sup>
GST-UbcH8	3.37	8	8919	41.604	41.737	42.842
UbcH8 dimer	4.402	6.2	5835	39.547	38.766	44.169

413 <sup>a</sup>Radius of gyration, <sup>b</sup>Maximum Dimension, <sup>c</sup>Porod Volume, <sup>d</sup>Molecular Weight, <sup>e</sup>Volume of

414 Correlation, <sup>f</sup>Porod invariant

415

416



417

418 **Supplementary Figure 1. Previously-determined Ubch8 crystal structures.** Cartoon and

419 surface representation of Ubch8 protein in the (A) dimeric form (PDB ID:1WZV) and (B)

420 monomeric form (PDB ID:1WZW)

421

